2020-09-30

Grainenergy release governs mobility of debris flow due to solidliquid mass release

Cao, Zhixian

http://hdl.handle.net/10026.1/17651

Grains-energy release governs mobility of debris flow due to solid-liquid mass release

Zhixian Cao[1], Ji Li[1], Alistair Borthwick[2], Qingquan Liu[3], Gareth Pender[4]

[1] State Key Laboratory of Water Resources and Hydropower Engineering Science, Wuhan University, Wuhan, China;

[2] Institute for Infrastructure and Environment, The University of Edinburgh, Edinburgh, UK;

[3] Department of Mechanics, Beijing Institute of Technology, Beijing , China;

[4] Institute for Infrastructure and Environment, Heriot-Watt University, Edinburgh, UK.

Correspondence

Zhixian Cao, State Key Laboratory of Water Resources and Hydropower Engineering Science, Wuhan University, Wuhan 430072, China.

Email: zxcao@whu.edu.cn

Qingquan Liu, Department of Mechanics, Beijing Institute of Technology, Beijing, 100081, China

Email: liuqq@bit.edu.cn

Content of this file

Text S1- Mathematical model

Consider debris flow over an erodible bed composed of non-cohesive sediments with N size classes. Let d_k denote the diameter of the k th sediment grain size, where subscript $k = 1, 2, ..., N$ reflecting the fact that debris flows are generally composed of multiple grain sizes, varying widely from clay (particle diameter $\approx 10^{-5}$ m) to boulders (particle diameter $\approx 10^1$ m) (Iverson, 1997). It should be noted that other existing depth-averaged models of debris flows, including quasi single-phase mixture models and two-phase models, are all confined to a single (representative) sediment size whose value is usually set constant as the median or mean sediment particle diameter. Inevitably, such existing models are oversimplified.

Based on continuum theory for both liquid (water) and solid (sediment) phases, a set of one-dimensional (1D) depth-averaged equations for mass and momentum conservation for the liquid-solid mixture, liquid, and solid phases over arbitrary slope is developed by transforming the basic three-dimensional two-phase flow equations (Pai, 1977) into a relatively simple set of equations. Following the conventional Reynolds averaging procedure, stresses due to fluctuations of liquid and solid motions are readily derived. Here "depth-averaged" refers to the fact that physical quantities (velocity and volume fraction) are integrated over the depth of the flow. Hence, vertical profiles of stress, velocity and volumetric sediment concentration are not resolved by the present depth-averaged two-phase model, unlike the vertical 1D model for steady and longitudinally uniform debris flows proposed by Egashira (2011). Physically, the solid

2

and liquid phases are assumed to be well mixed through the depth of a debris flow, and so it is difficult to identify the flow structure of an upper pure liquid layer overlaying a solid-liquid mixture layer, as opposed to subaqueous turbidity currents in open channels, which flow under a pure water flow layer (Cao et al., 2015), for which a double layer-averaged model is warranted. Moreover, the shape factors, which arise from the depth-averaging procedure and represent the effects of non-uniformity in vertical structure of the velocity and sediment concentration profiles, are presumed to be unity. This conventional practice in shallow water-sediment flow models (Wu, 2007), implies the effect of shape factors may be neglected. However, this does not actually mean that the velocity and sediment concentration have to be constant over the flow depth. A detailed derivation of the governing equations is given in the Supplementary materials file of Li et al. (2018a). Essentially, the governing equations comprise mass and momentum conservation equations for the liquid-solid mixture, the solid phase, and the liquid phase, and global mass conservation equations for the bed sediment. When formulating the mathematical model for a debris flow over an erodible bed, only two of the three governing equation systems for the liquid-solid mixture are used. Following Li et al. (2018a, b), the governing equation system for debris flow is composed of equations for the liquid-solid mixture and the sediment phase because the resulting system is hyperbolic and characterized by straightforward derivation of real, distinct eigenvalues.

The depth-averaged mass and momentum conservation equations for the liquid-solid mixture are

$$\frac{\partial}{\partial t}\rho_m h + \frac{\partial}{\partial x}\rho_m h U_m = -\rho_0 \frac{\partial z_b}{\partial t} \tag{S1}$$

and

$$\frac{\partial \rho_m h U_m}{\partial t} + \frac{\partial}{\partial x}(\rho_m h U_m^2 + \frac{1}{2}\rho_m g'h^2) = \rho_m gh\sin\theta - \tau_b - \rho_m g'h\frac{\partial z_b}{\partial x}$$
$$+ \frac{\partial}{\partial x}[hT_R + hT_\mu] - \frac{\partial}{\partial x}h\sum[\rho_s C_k i_{s_k}(i_{s_k} - i_f)] \tag{S2}$$

The depth-averaged mass and momentum conservation equations for the solid phase are

$$\frac{\partial \rho_s h C_k}{\partial t} + \frac{\partial \rho_s h C_k U_{sk}}{\partial x} = \rho_s F_k \tag{S3}$$

$$\frac{\partial \rho_s h C_k U_{sk}}{\partial t} + \frac{\partial}{\partial x}(\rho_s h C_k U_{sk}^2 + \frac{1}{2}C_k \rho_m g'h^2) = \rho_s gh C_k \sin\theta - \tau_{s_k b} - \rho_m g'h C_k \frac{\partial z_b}{\partial x}$$
$$+ F_{s_k f} + F_{s-s_k} + \frac{\partial}{\partial x}(h C_k T_{Rs_k} + h C_k T_{\mu s_k}) \tag{S4}$$
$$+ \frac{1}{2}\rho_m g'h^2 \frac{\partial C_k}{\partial x}$$

The bed deformation equation is

$$\frac{\partial z_b}{\partial t} = -\sum \frac{F_k}{1-p} \tag{S6}$$

where t is time, x is stream-wise distance parallel to the bed slope, θ is the angle of bed slope, such that $g' = g\cos\theta$, the subscripts s and m denote the solid phase and the liquid-solid mixture, h is the debris flow depth and z_b is the bed elevation (both in the direction normal to the substrate surface), C_k is the depth-averaged size-specific volumetric sediment concentration, $C_T = \sum C_k$ is the depth-averaged total sediment concentration, ρ_f and ρ_s are the densities of the liquid and solid phases respectively, $\rho_m = \rho_s C_T + \rho_f (1 - C_T)$ is the density of the liquid-solid mixture;

$\rho_0 = \rho_f \theta_f + \rho_s(1-p)$ is the bed density, p is the bed sediment porosity (with $1-p$ the volumetric sediment concentration of the stationary bed), θ_f is the water content of the bed (normally $\theta_f \leq p$), U_{sk} is the size-specific depth-averaged velocity of the solid phase in the $x-$ direction, U_m is the depth-averaged velocity of the liquid-solid mixture in the $x-$ direction; $i_{s_k} = U_{sk} - U_m$ denotes the difference between the size-specific solid phase velocity U_{sk} and the liquid-solid mixture velocity U_m, τ_b and $\tau_{s_k b}$ are bed shear stresses for the liquid-solid mixture and the solid phases in the $x-$ direction, T_R and T_{Rs_k} are depth-averaged stresses for the liquid-solid mixture and solid phases respectively due to fluctuations of the liquid and solid motions in the $x-$ direction; T_μ and $T_{\mu s_k}$ are depth-averaged viscous stresses for the liquid-solid mixture and solid phases in the $x-$ direction, $F_{s_k f}$ is the size-specific depth-averaged interphase interaction force, F_{s-s_k} is the size-specific depth-averaged particle-particle interaction drag force (which is exerted on solid phase k by the other constituents of solid phase and such that $\sum(F_{s-s_k}) = 0$), F_k is the size-specific net flux of sediment exchange between the flow and the bed, and $F_T = \sum F_k$.

For multiple grain sizes, the active layer concept due to Hirano (1971), which has been widely used in the context of fluvial hydraulics (Wu, 2007), is adopted to resolve bed grain size stratigraphic evolution. By analogy to fluvial hydraulics (Hirano, 1971; Parker, 1991a, b), the model is virtually based on a three-layer structure, composed of the debris flow layer, the active layer, and the substrate layer. The active layer is located between the debris flow layer and the substrate layer. Sediments within the active layer are assumed to be well mixed in the vertical and can exchange freely with the upper

5

and lower layers. The substrate layer, known as the stratigraphy of the deposit, has certain structure and may vary in time. Physically, the active layer equation is based on the size-specific mass conservation of bed sediments. In general, three critical parameters are involved, i.e., the active layer thickness, the size-specific sediment exchange between the debris flow and the bed, and the sediment fraction at the lower interface of the active layer. Accordingly, the active layer equation is

$$\frac{\partial h_a f_{ak}}{\partial t} + f_{Ik} \frac{\partial \xi}{\partial t} = -\frac{F_k}{1-p} \tag{S7}$$

where h_a is the thickness of the active layer, f_{ak} is the fraction of the k th size sediment in the active layer and $\sum f_{ak} = 1$, $\xi = z_b - h_a$ is the elevation of the bottom surface of the active layer, and f_{Ik} is the fraction of the k th size sediment in the interface between the active layer and the substrate layer, whereby $\sum f_{Ik} = 1$. In the present study, the active layer thickness is set such that $h_a = 2d_{84}$ following the convention in fluvial hydraulics (Hoey & Ferguson, 1994), where $d_{84} =$ particle size at which 84% of the sediment is finer. It can be seen from Eq. (S7) that the net flux of sediment exchange [i.e., the right hand side (RHS) of Eq. (S7)] is balanced by the variation in the fraction of the active layer [i.e., the first term on the left hand side (LHS) of Eq. (S7)] and the change in sediment content due to movement of the interface between the active layer and its substrate [i.e., the second term on the LHS of Eq. (S7)]. Moreover, the bed deformation equation, i.e., Eq. (S6) can be readily obtained by integrating Eq. (S7) over all grain sizes, because $\sum f_{ak} = 1$ and $\sum f_{Ik} = 1$.

Physically, mass exchange between the debris flow and the bed does not involve any momentum exchange. This is justified because the flow momentum cannot change

6

because sediment and water entrained from the static bed do not have any initial momentum. Likewise, the flow momentum does not vary due to the sediment deposited onto the bed (Cao et al., 2017). This proposition is well established, and has been applied in previous models of fluvial processes (e.g., Cao et al., 2004; Wu, 2007; Qian et al., 2015, 2017) and earth surface flows such as debris flows (Bridge & Demicco, 2008; Li et al., 2018a). However, this is not the case in the liquid-solid mixture momentum equation reformulated by Iverson and Ouyang (2015) and applied by Ouyang et al. (2015). Specifically, an extra term "$\rho_m F_T U_b$", denoting momentum exchange between the flow and the static bed, was added into the momentum conservation equation of these models in the $x-$ direction and its counterpart in the $y-$ direction, where U_b is the flow velocity at the bottom boundary and is assumed to be equal to the depth-averaged flow velocity U_m. The extra term produces momentum gain (when $F_T > 0$) or loss (when $F_T < 0$), and stems from the way the boundary condition is characterized. However, the velocity components must vanish physically at the bed surface because the bed is static, commonly known as the no-slip condition of a viscous fluid, i.e., $U_b = 0$. Moreover, this term can cause the model to crash (Cao et al., 2017).

References in Text S1

Bridge, J., & Demicco, R. (2008). *Earth surface processes, landforms and sediment deposits*. Cambridge University Press: Cambridge.

Cao, Z., Li, J., Pender, G., & Liu, Q. (2015). Whole-process modeling of reservoir turbidity currents by a double layer-averaged model. *Journal of Hydraulic Engineering*, *141*(2), 04014069. doi: 10.1061/(ASCE)HY.1943-7900.0000951.

Cao, Z., Pender, G., Wallis, S., & Carling, P. (2004). Computational dam-break hydraulics over erodible sediment bed. *Journal of Hydraulic Engineering*, *130*(7), 689-703. doi: 10.1061/(ASCE)0733-9429(2004)130:7(689).

Cao, Z., Xia, C., Pender, G., & Liu, Q. (2017). Shallow water hydro-sediment-morphodynamic equations for fluvial processes. *Journal of Hydraulic Engineering*, Forum Article. doi:10.1061/(ASCE)HY.1943-7900.0001281.

Egashira, S. (2011). Prospects of debris flow studies from constitutive relations to governing equations. *Journal of Disaster Research*, *6*(3): 313-320. doi: 10.20965/jdr.2011.p0313.

Hirano, M. (1971). River bed degradation with armouring. *Transactions of Japanese Society of Civil Engineering*, *195*(11), 55-65 (in Japanese).

Hoey, T. B., & Ferguson, R. (1994). Numerical simulation of downstream fining by selective transport in gravel bed rivers: Model development and illustration. *Water Resource Research*, *30*(7), 2251–2260. doi:10.1029/94WR00556.

Iverson, R. M. (1997). The physics of debris flows. *Reviews of geophysics*, *35*(3), 245-296. doi: 10.1029/97RG00426.

Iverson, R. M., & Ouyang, C. (2015). Entrainment of bed material by earth surface mass flows: Review and reformulation of depth-integrated theory. *Reviews of*

Geophysics, *53*(1), 27-58. doi: 10.1002/2013RG000447.

Li, J., Cao, Z., Hu, K., Pender, G., & Liu, Q. (2018a). A depth-averaged two-phase model for debris flows over erodible bed. *Earth Surface Processes and Landforms*, *43*(4), 817-839. doi: 10.1002/esp.4283.

Li, J., Cao, Z., Hu, K., Pender, G., & Liu, Q. (2018b). A depth-averaged two-phase model for debris flows over fixed beds. *International Journal of Sediment Research*, *33*(4), 462-477. doi: 10.1016/j.ijsrc.2017.06.003.

Ouyang, C., He, S., & Tang, C. (2015). Numerical analysis of dynamics of debris flow over erodible beds in Wenchuan earthquake-induced area. *Engineering Geology*, *194*, 62-72. doi: 10.1016/j.enggeo.2014.07.012.

Pai, S. I. (1977). *Two-phase flows*. Berlin: Springer-Verlag.

Parker G. 1991a. Selective Sorting and Abrasion of River Gravel. I: Theory. *Journal of Hydraulic Engineering*, *117*, 131-147, doi: 10.1061/(ASCE)0733-9429(1991)117:2(131).

Parker G. 1991b. Selective Sorting and Abrasion of River Gravel. II: Applications. *Journal of Hydraulic Engineering*, *117*, 150-171, doi: 10.1061/(ASCE)0733-9429(1991)117:2(150).

Qian, H., Cao, Z., Pender, G., Liu, H., & Hu, P. (2015). Well-balanced numerical modeling of non-uniform sediment transport in alluvial rivers. *International Journal of Sediment Research*, *30*(2), 117-130. doi: 10.1016/j.ijsrc.2015.03.002.

Qian, H., Cao, Z., Liu, H., & Pender, G. (2017). Numerical modelling of alternate bar formation, development and sediment sorting in straight channels. *Earth Surface Processes and Landforms*, 42(4), 555-574. doi: 10.1002/esp.3988.

Wu, W. (2007). *Computational river dynamics*. London: Taylor & Francis.
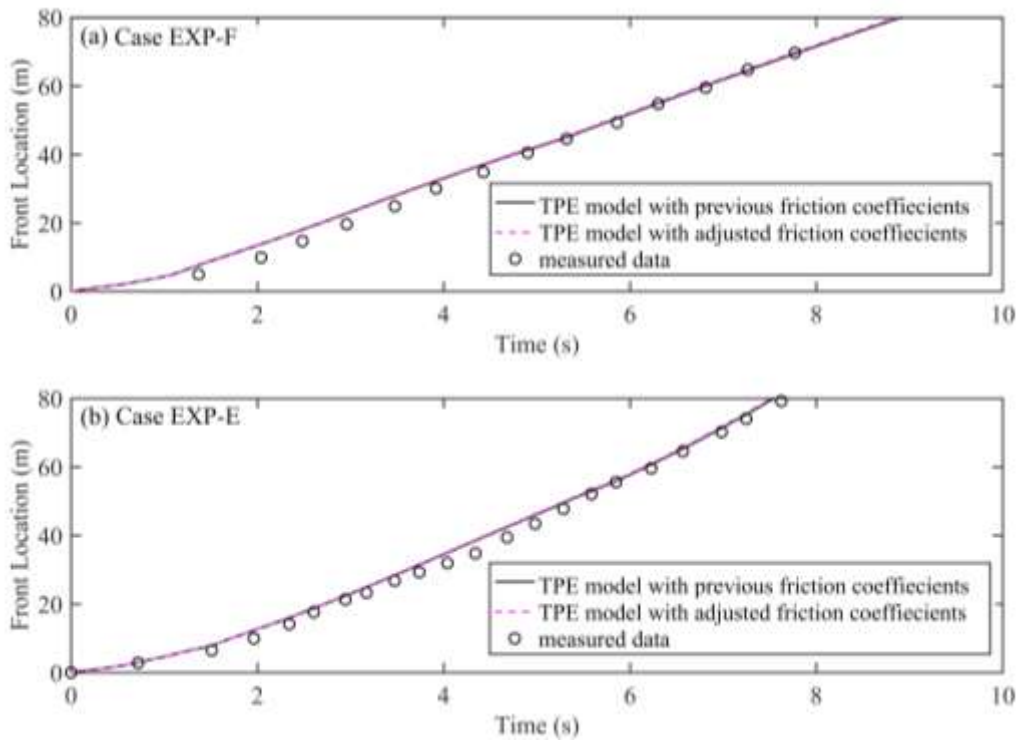
FIGURE S1 Front location time histories: predicted using a depth-averaged two-phase equation (TPE) model with previous friction coefficients (Li et al., 2018a) (solid line) and adjusted friction coefficients (dashed line), and measured data (Iverson et al., 2011) (open circles). (a) Debris flow over a fixed bed (i.e., Case EXP-F). (b) Debris flow over an erodible bed (i.e., Case EXP-E).
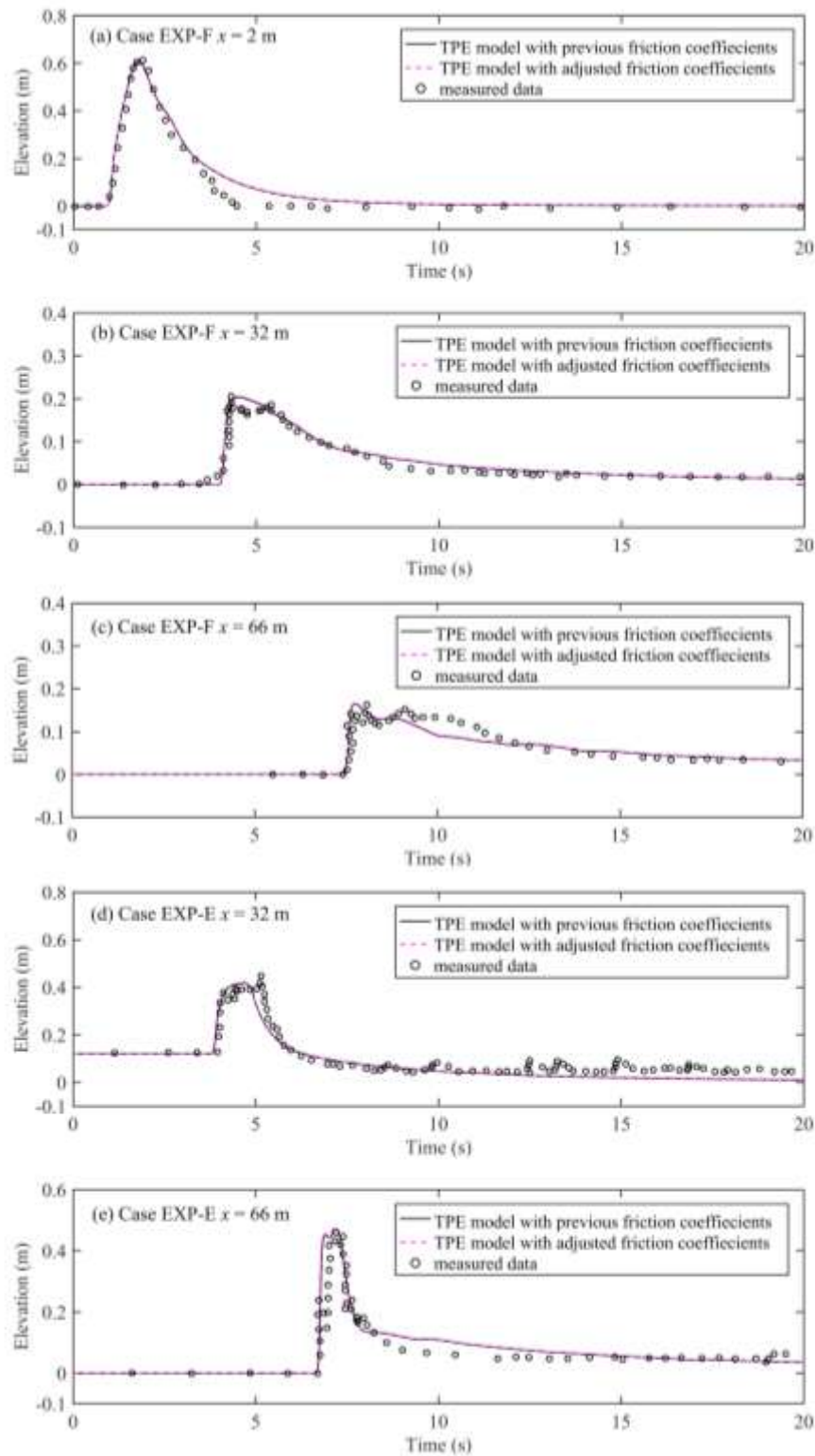
FIGURE S2 Time histories of flow surface elevation above the bed: predicted by a depth-averaged two-phase equation (TPE) model with previous friction coefficients (Li et al., 2018a) (solid line) and adjusted friction coefficients (dashed line), and measured data (Iverson et al., 2011) (open circles). (a-c) Debris flow over fixed bed at $x = $ 2, 32, and 66 m respectively. (d-e) Debris flow over erodible bed at $x = $ 32 and 66 m.
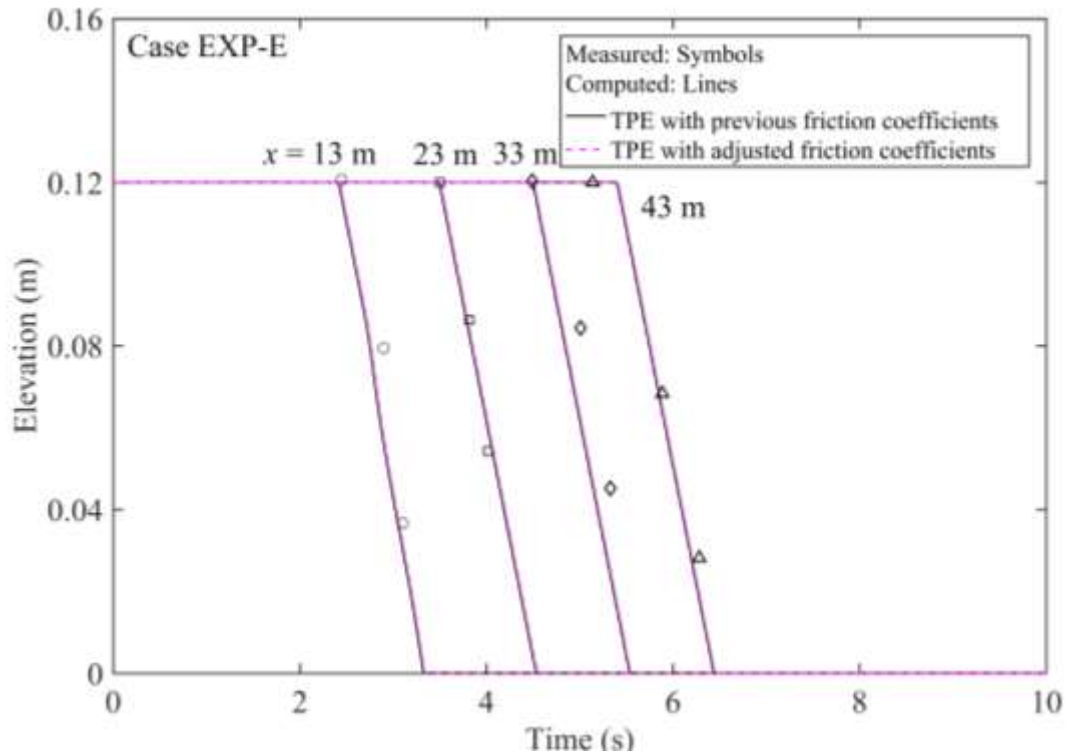
FIGURE S3 Bed elevation time histories at x = 13, 23, 33, and 43 m for Case EXP-E: predicted by a depth-averaged two-phase equation (TPE) model with previous friction coefficients (Li et al., 2018a) (solid line) and adjusted friction coefficients (dashed line), and measured data (Iverson et al., 2011) (open circles).
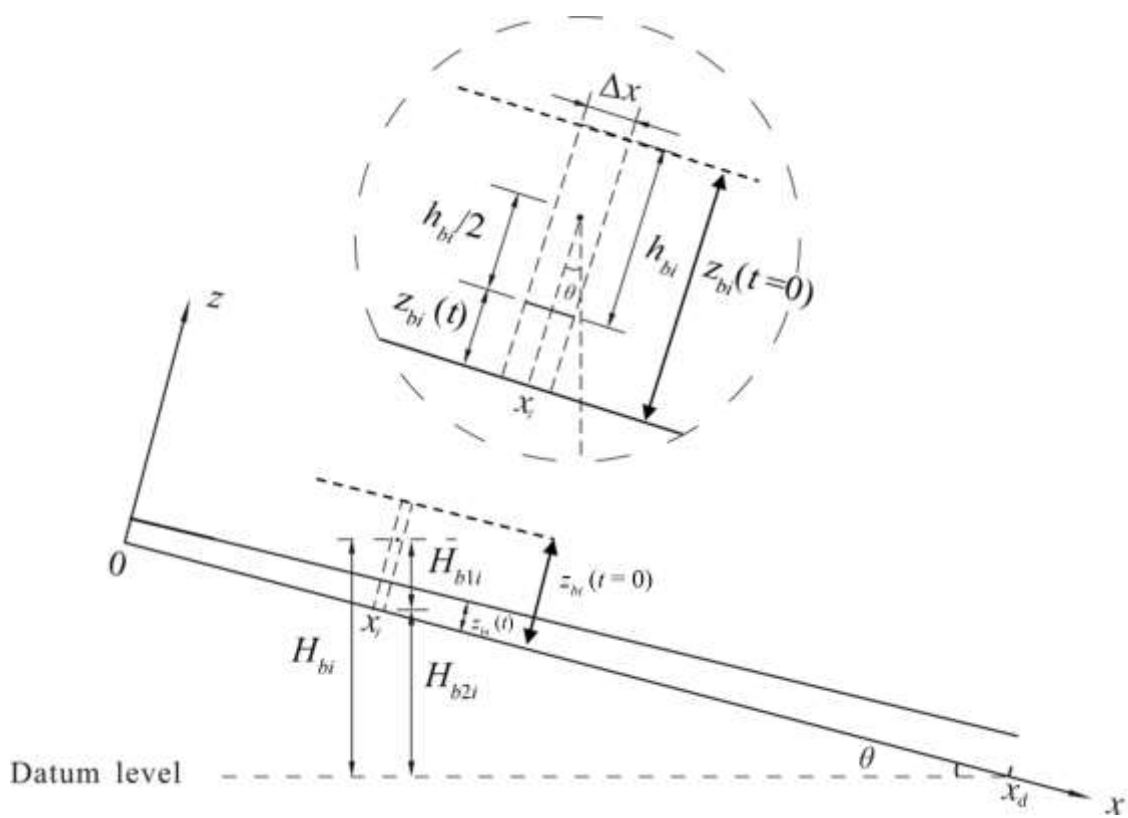
Figure S4 Sketch of control volume used for calculation of potential energy due to sediment exchange with the bed.
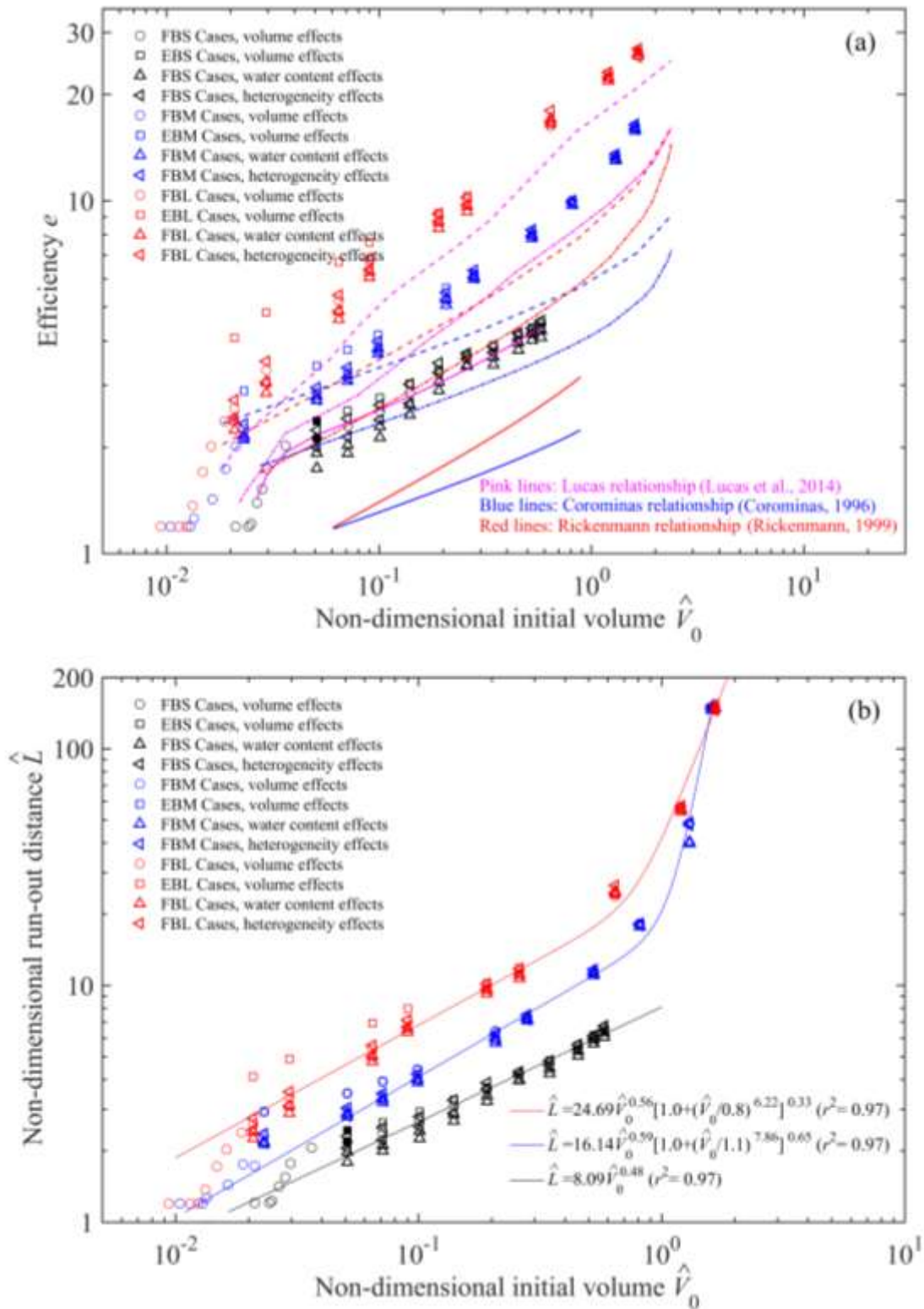
FIGURE S5 Dependence of debris flow mobility on initial volume over a 40° sloping ramp. (a) Efficiency against non-dimensional initial volume. Solid, dotted and dashed lines respectively present the empirical results for laboratory-scale, intermediate and large field-scale cases. (b) Run-out distance against non-dimensional initial volume.
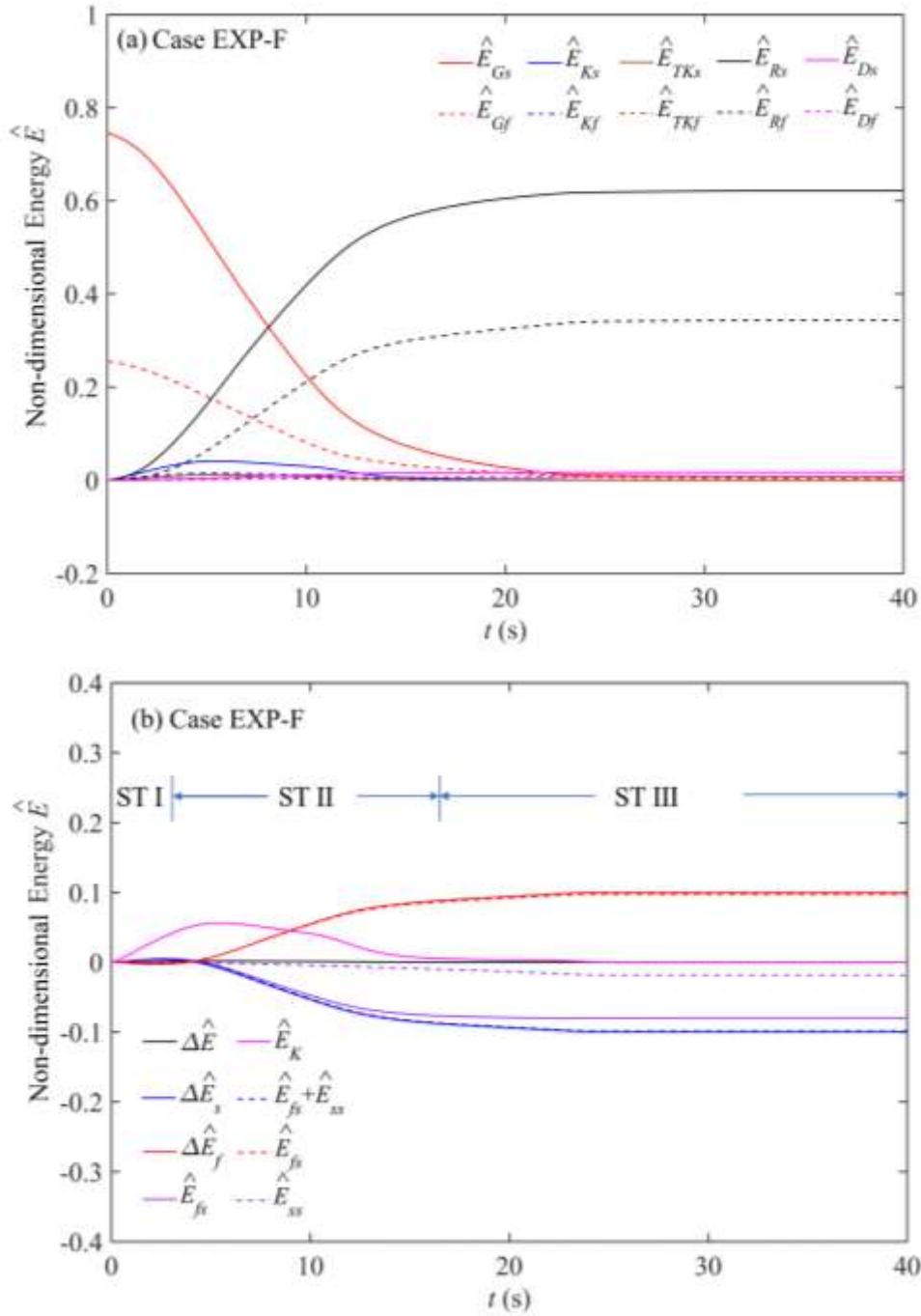
FIGURE S6 Evolution of energy components and energy changes in USGS experimental fixed-bed debris flows (Iverson et al., 2011). (a) Evolution of non-dimensional energy components, including kinetic energy ($\hat{E}_K$), fluctuation kinetic energy ($\hat{E}_{TK}$), gravitational potential energy ($\hat{E}_G$), and energy dissipation due to bed resistance ($\hat{E}_R$) and fluctuation motions ($\hat{E}_D$). (b) Evolution of non-dimensional energy changes of the solid-liquid mixture ($\Delta\hat{E}$), the solid phase ($\Delta\hat{E}_s$), the liquid phase ($\Delta\hat{E}_f$) as well as the the work done by inter-phase ($\hat{E}_{fs}$ and $\hat{E}_{sf}$) and inter-grain size interaction forces ($\hat{E}_{ss}$)
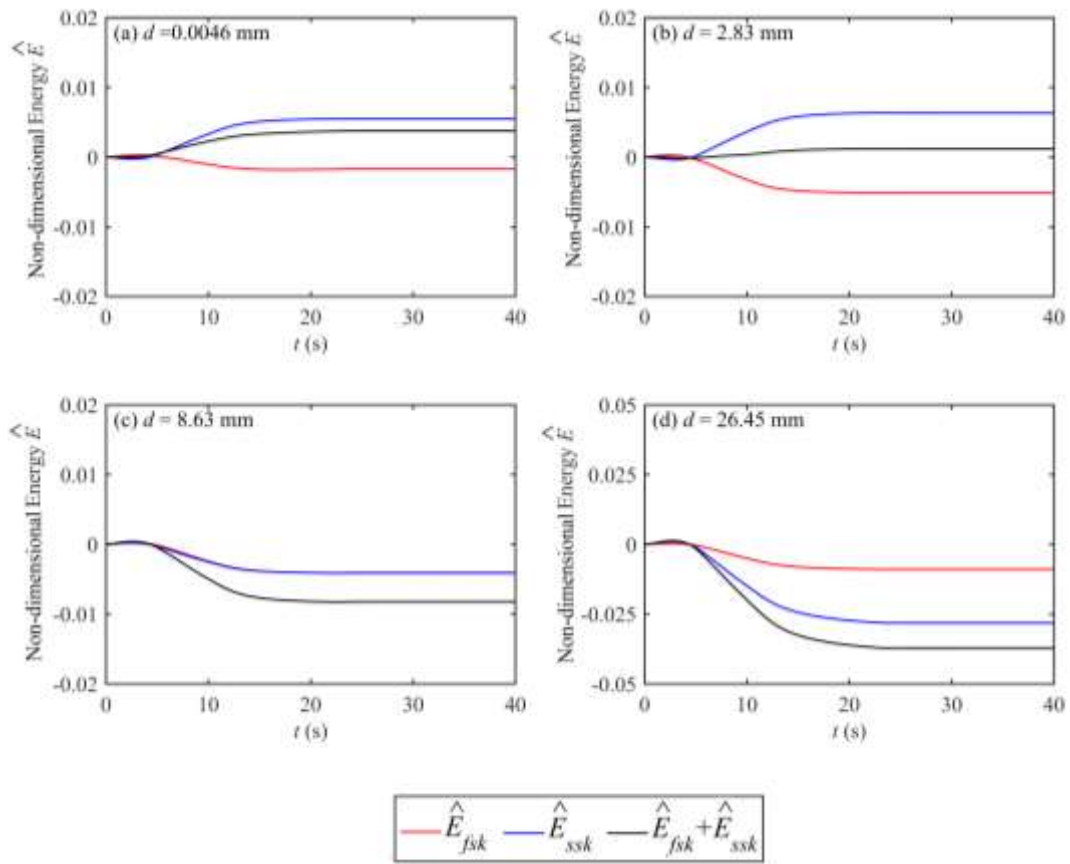
FIGURE S7 Evolution of non-dimensional energy changes in size-specific grains for Case EXP-F. (a-b) fine grains; (c-d) coarse grains. $\hat{E}_{fsk}$ and $\hat{E}_{sfk}$ represent work done by the inter-phase interaction force components, and $\hat{E}_{ssk}$ represents work done by the inter-grain size interaction force.
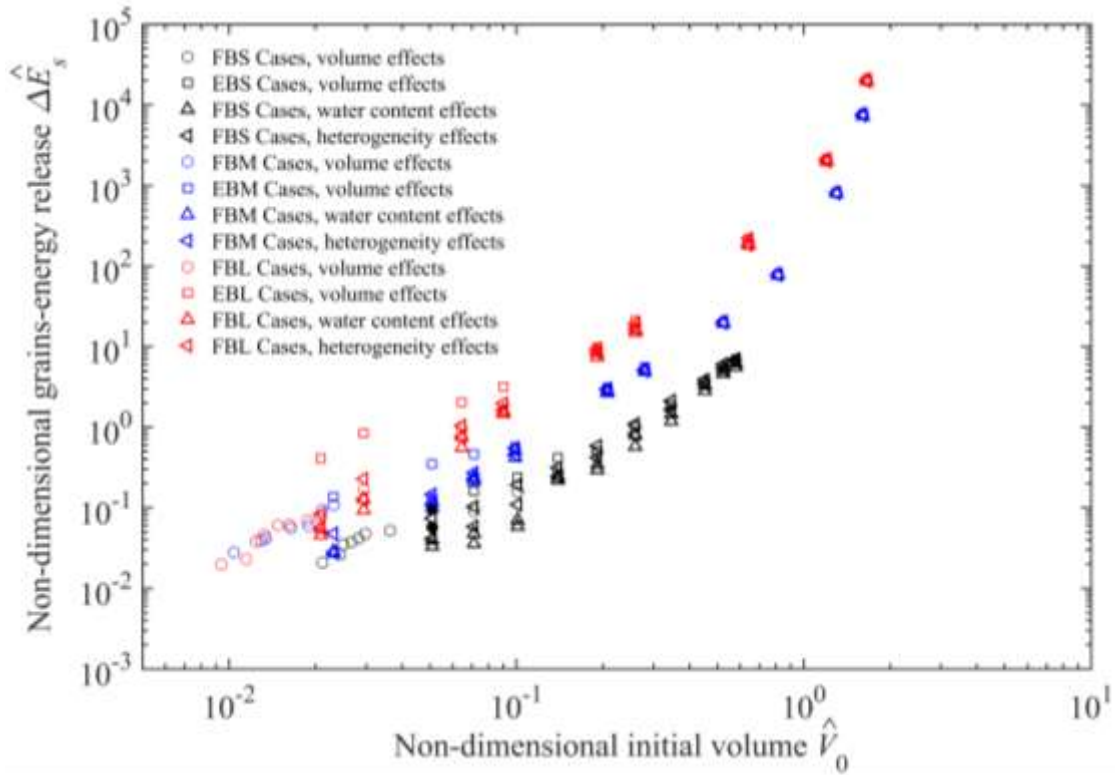
FIGURE S8 Dependence of grains-energy release on initial debris flow volume over a 40° sloping ramp.
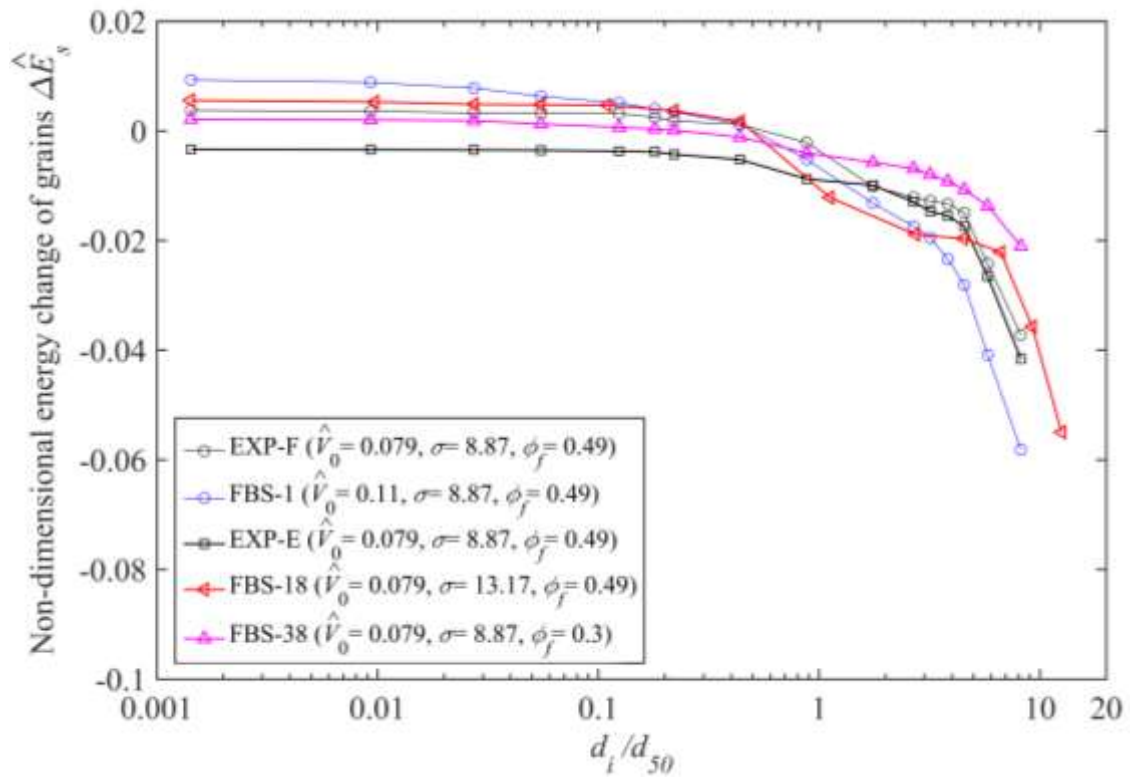
FIGURE S9 Energy changes of size-specific grains at debris flow stoppage.

17

TABLE S1 Material composition of SGM

	SGM (Sand-Gravel-Mud)	
Number	d (mm)	Percent (%)
1	0.0046	3.92
2	0.03	3.52
3	0.088	3.04
4	0.177	6.45
5	0.4	6.0
6	0.42	6.5
7	0.71	8.95
8	1.41	6.25
8	2.83	8.31
10	5.65	6.05
11	8.63	5.0
12	10.27	6.38
13	12.34	6.02
14	14.67	6.05
15	18.7	7.95
16	26.45	9.98

TABLE S2 Summary of USGS debris flow experiments and results

Notation	V_0 (m³)	σ	ϕ_f	θ (°)	e	$\hat{L}$	$\Delta\hat{E}_s$
EXP-F	6	8.87	0.49	31	2.030	2.09	0.046
EXP-E	6	8.87	0.49	31	2.263	2.33	0.077

TABLE S3 Summary of laboratory-scale numerical cases and results

Notation	V_0 (m³)	σ	ϕ_f	θ (°)	e	$\hat{L}$	$\Delta\hat{E}_s$
FBS Cases ($b =$ 2 m)							
FBS-1	12	8.87	0.49	31	2.165	2.26	0.07
FBS-2	25	8.87	0.49	31	2.389	2.54	0.13
FBS-3	50	8.87	0.49	31	2.683	2.92	0.22
FBS-4	100	8.87	0.49	31	3.060	3.44	0.39
FBS-5	200	8.87	0.49	31	3.380	3.98	0.80
FBS-6	400	8.87	0.49	31	3.576	4.47	1.45
FBS-7	800	8.87	0.49	31	3.852	5.22	2.92
FBS-8	1200	8.87	0.49	31	4.013	5.76	4.44
FBS-9	1600	8.87	0.49	31	4.165	6.25	5.42
FBS-10	2	8.87	0.49	31	1.664	1.69	0.02
FBS-11	2.5	8.87	0.49	31	1.664	1.70	0.02
FBS-12	3	8.87	0.49	31	1.664	1.70	0.03
FBS-13	3.5	8.87	0.49	31	1.725	1.77	0.03
FBS-14	4	8.87	0.49	31	1.825	1.87	0.03
FBS-15	4.5	8.87	0.49	31	1.868	1.92	0.04
FBS-16	5	8.87	0.49	31	1.925	1.98	0.04
FBS-17	6	4.25	0.49	31	1.930	1.99	0.03
FBS-18	6	13.17	0.49	31	2.150	2.22	0.06
FBS-19	12	4.25	0.49	31	2.025	2.11	0.05
FBS-20	12	13.17	0.49	31	2.282	2.38	0.08
FBS-21	25	4.25	0.49	31	2.255	2.40	0.09
FBS-22	25	13.17	0.49	31	2.490	2.65	0.15
FBS-23	50	4.25	0.49	31	2.501	2.72	0.20
FBS-24	50	13.17	0.49	31	2.835	3.09	0.25
FBS-25	100	4.25	0.49	31	2.865	3.22	0.33
FBS-26	100	13.17	0.49	31	3.256	3.66	0.46
FBS-27	200	4.25	0.49	31	3.165	3.73	0.65
FBS-28	200	13.17	0.49	31	3.465	4.08	0.87
FBS-29	400	4.25	0.49	31	3.476	4.35	1.30
FBS-30	400	13.17	0.49	31	3.635	4.55	1.68
FBS-31	800	4.25	0.49	31	3.764	5.10	2.71
FBS-32	800	13.17	0.49	31	3.942	5.34	3.06
FBS-33	1200	4.25	0.49	31	3.925	5.63	4.19
FBS-34	1200	13.17	0.49	31	4.056	5.82	4.74
FBS-35	1600	4.25	0.49	31	4.086	6.14	5.18
FBS-36	1600	13.17	0.49	31	4.256	6.39	5.49
FBS-37	6	8.87	0.1	31	1.690	1.74	0.03
FBS-38	6	8.87	0.3	31	1.856	1.91	0.03

FBS-39	12	8.87	0.1	31	1.819	1.90	0.03
FBS-40	12	8.87	0.3	31	1.918	2.00	0.04
FBS-41	25	8.87	0.1	31	2.012	2.14	0.05
FBS-42	25	8.87	0.3	31	2.160	2.30	0.06
FBS-43	50	8.87	0.1	31	2.325	2.53	0.18
FBS-44	50	8.87	0.3	31	2.478	2.70	0.20
FBS-45	100	8.87	0.1	31	2.725	3.07	0.24
FBS-46	100	8.87	0.3	31	2.875	3.24	0.27
FBS-47	200	8.87	0.1	31	3.036	3.57	0.46
FBS-48	200	8.87	0.3	31	3.189	3.75	0.64
FBS-49	400	8.87	0.1	31	3.215	4.02	0.95
FBS-50	400	8.87	0.3	31	3.368	4.21	1.16
FBS-51	800	8.87	0.1	31	3.526	4.78	2.25
FBS-52	800	8.87	0.3	31	3.702	5.02	2.61
FBS-53	1200	8.87	0.1	31	3.756	5.39	3.64
FBS-54	1200	8.87	0.3	31	3.913	5.61	4.04
FBS-55	1600	8.87	0.1	31	3.825	5.74	4.43
FBS-56	1600	8.87	0.3	31	3.992	5.99	4.89
FBS-57	6	8.87	0.49	40	2.121	2.18	0.06
FBS-58	12	8.87	0.49	40	2.293	2.39	0.09
FBS-59	25	8.87	0.49	40	2.533	2.68	0.16
FBS-60	50	8.87	0.49	40	2.857	3.10	0.28
FBS-61	100	8.87	0.49	40	3.262	3.65	0.49
FBS-62	200	8.87	0.49	40	3.611	4.22	1.00
FBS-63	400	8.87	0.49	40	3.823	4.73	1.82
FBS-64	800	8.87	0.49	40	4.115	5.50	3.68
FBS-65	1200	8.87	0.49	40	4.300	6.07	5.60
FBS-66	1600	8.87	0.49	40	4.475	6.60	6.84
FBS-67	1	8.87	0.49	40	1.192	1.21	0.02
FBS-68	1.33	8.87	0.49	40	1.192	1.21	0.03
FBS-69	1.4	8.87	0.49	40	1.213	1.23	0.04
FBS-70	1.6	8.87	0.49	40	1.392	1.41	0.04
FBS-71	1.8	8.87	0.49	40	1.522	1.55	0.04
FBS-72	2	8.87	0.49	40	1.739	1.77	0.05
FBS-73	3	8.87	0.49	40	2.017	2.06	0.05
FBS-74	6	4.25	0.49	40	1.999	2.06	0.04
FBS-75	6	13.17	0.49	40	2.237	2.30	0.07
FBS-76	12	4.25	0.49	40	2.139	2.23	0.06
FBS-77	12	13.17	0.49	40	2.411	2.51	0.10
FBS-78	25	4.25	0.49	40	2.389	2.53	0.11
FBS-79	25	13.17	0.49	40	2.635	2.79	0.19
FBS-80	50	4.25	0.49	40	2.659	2.88	0.24
FBS-81	50	13.17	0.49	40	3.018	3.27	0.31
FBS-82	100	4.25	0.49	40	3.252	3.64	0.42

FBS-83	100	13.17	0.49	40	3.465	3.88	0.58
FBS-84	200	4.25	0.49	40	3.566	4.17	0.82
FBS-85	200	13.17	0.49	40	3.689	4.31	1.09
FBS-86	400	4.25	0.49	40	3.707	4.59	1.63
FBS-87	400	13.17	0.49	40	3.877	4.80	2.11
FBS-88	800	4.25	0.49	40	4.018	5.37	3.41
FBS-89	800	13.17	0.49	40	4.207	5.62	3.85
FBS-90	1200	4.25	0.49	40	4.202	5.93	5.28
FBS-91	1200	13.17	0.49	40	4.345	6.13	5.99
FBS-92	1600	4.25	0.49	40	4.374	6.45	6.54
FBS-93	1600	13.17	0.49	40	4.566	6.74	6.98
FBS-94	6	8.87	0.1	40	1.744	1.79	0.03
FBS-95	6	8.87	0.3	40	1.926	1.98	0.04
FBS-96	12	8.87	0.1	40	1.922	2.00	0.04
FBS-97	12	8.87	0.3	40	2.027	2.11	0.05
FBS-98	25	8.87	0.1	40	2.132	2.26	0.06
FBS-99	25	8.87	0.3	40	2.290	2.43	0.07
FBS-100	50	8.87	0.1	40	2.470	2.68	0.22
FBS-101	50	8.87	0.3	40	2.637	2.86	0.25
FBS-102	100	8.87	0.1	40	2.898	3.24	0.29
FBS-103	100	8.87	0.3	40	3.061	3.42	0.34
FBS-104	200	8.87	0.1	40	3.418	3.99	0.58
FBS-105	200	8.87	0.3	40	3.395	3.97	0.80
FBS-106	400	8.87	0.1	40	3.431	4.25	1.19
FBS-107	400	8.87	0.3	40	3.604	4.46	1.46
FBS-108	800	8.87	0.1	40	3.768	5.03	2.83
FBS-109	800	8.87	0.3	40	3.954	5.28	3.28
FBS-110	1200	8.87	0.1	40	4.021	5.68	4.59
FBS-111	1200	8.87	0.3	40	4.192	5.92	5.10
FBS-112	1600	8.87	0.1	40	4.095	6.04	5.59
FBS-113	1600	8.87	0.3	40	4.283	6.32	6.21
EBS Cases ($V_b = $ 10.9 m^3, $b = $ 2 m)							
EBS-1	12	8.87	0.49	31	2.422	2.53	0.12
EBS-2	25	8.87	0.49	31	2.628	2.79	0.17
EBS-3	50	8.87	0.49	31	2.850	3.10	0.24
EBS-4	100	8.87	0.49	31	3.120	3.51	0.41
EBS-5	200	8.87	0.49	31	3.420	4.03	0.81
EBS-6	400	8.87	0.49	31	3.640	4.55	1.50
EBS-7	800	8.87	0.49	31	3.920	5.31	2.98
EBS-8	1200	8.87	0.49	31	4.100	5.88	4.44
EBS-9	1600	8.87	0.49	31	4.200	6.31	5.44
EBS-10	6	8.87	0.49	40	2.373	2.44	0.09
EBS-11	12	8.87	0.49	40	2.535	2.64	0.16
EBS-12	25	8.87	0.49	40	2.759	2.92	0.24

EBS-13	50	8.87	0.49	40	3.025	3.28	0.41
EBS-14	100	8.87	0.49	40	3.312	3.71	0.50
EBS-15	200	8.87	0.49	40	3.659	4.27	1.01
EBS-16	400	8.87	0.49	40	3.886	4.81	1.85
EBS-17	800	8.87	0.49	40	4.173	5.58	3.70
EBS-18	1200	8.87	0.49	40	4.367	6.16	5.65
EBS-19	1600	8.87	0.49	40	4.499	6.64	6.90

TABLE S4 Summary of intermediate field-scale cases and results

				FBM Cases ($b =$ 20 m)			
Notation	V_0 (m³)	σ	ϕ_f	θ (°)	e	$\hat{L}$	$\Delta\hat{E}_s$
FBM-1	300	8.87	0.49	31	2.042	2.07	0.03
FBM-2	600	8.87	0.49	31	2.182	2.22	0.06
FBM-3	1500	8.87	0.49	31	2.568	2.65	0.12
FBM-4	3000	8.87	0.49	31	2.925	3.05	0.24
FBM-5	6000	8.87	0.49	31	3.468	3.68	0.49
FBM-6	1.5×10^4	8.87	0.49	31	4.126	4.53	1.20
FBM-7	3.0×10^4	8.87	0.49	31	4.725	5.37	2.73
FBM-8	6.0×10^4	8.87	0.49	31	5.523	6.60	4.75
FBM-9	1.5×10^5	8.87	0.49	31	6.349	8.30	9.02
FBM-10	3.0×10^5	8.87	0.49	31	7.250	10.40	18.59
FBM-11	6.0×10^5	8.87	0.49	31	7.952	12.84	36.82
FBM-12	1.2×10^6	8.87	0.49	31	8.925	16.68	72.53
FBM-13	6.0×10^6	8.87	0.49	31	10.365	30.50	373.72
FBM-14	1.2×10^7	8.87	0.49	31	11.625	43.57	725.30
FBM-15	6.0×10^7	8.87	0.49	31	14.020	100.16	3598.81
FBM-16	1.2×10^8	8.87	0.49	31	14.960	123.21	7169.93
FBM-17	30	8.87	0.49	31	1.664	1.67	0.02
FBM-18	50	8.87	0.49	31	1.664	1.67	0.02
FBM-19	100	8.87	0.49	31	1.664	1.68	0.02
FBM-20	152.5	8.87	0.49	31	1.664	1.68	0.02
FBM-21	175	8.87	0.49	31	1.795	1.81	0.03
FBM-22	250	8.87	0.49	31	1.915	1.94	0.03
FBM-23	300	4.25	0.49	31	1.922	1.95	0.03
FBM-24	300	13.17	0.49	31	2.125	2.15	0.05
FBM-25	600	4.25	0.49	31	2.087	2.13	0.05
FBM-26	600	13.17	0.49	31	2.285	2.33	0.07
FBM-27	1500	4.25	0.49	31	2.456	2.53	0.10
FBM-28	1500	13.17	0.49	31	2.657	2.74	0.14
FBM-29	3000	4.25	0.49	31	2.829	2.95	0.21
FBM-30	3000	13.17	0.49	31	3.027	3.16	0.25
FBM-31	6000	4.25	0.49	31	3.355	3.56	0.42
FBM-32	6000	13.17	0.49	31	3.593	3.81	0.51
FBM-33	1.5×10^4	4.25	0.49	31	4.027	4.42	1.09
FBM-34	1.5×10^4	13.17	0.49	31	4.271	4.69	1.31
FBM-35	3.0×10^4	4.25	0.49	31	4.662	5.30	2.66
FBM-36	3.0×10^4	13.17	0.49	31	4.901	5.57	2.78
FBM-37	6.0×10^4	4.25	0.49	31	5.405	6.46	4.63
FBM-38	6.0×10^4	13.17	0.49	31	5.661	6.76	4.84
FBM-39	1.5×10^5	4.25	0.49	31	6.234	8.15	8.95
FBM-40	1.5×10^5	13.17	0.49	31	6.478	8.47	9.15

FBM-41	$3.0×10^5$	4.25	0.49	31	7.132	10.23	18.31
FBM-42	$3.0×10^5$	13.17	0.49	31	7.402	10.62	18.77
FBM-43	$6.0×10^5$	4.25	0.49	31	7.725	12.47	36.26
FBM-44	$6.0×10^5$	13.17	0.49	31	8.057	13.01	37.10
FBM-45	$1.2×10^6$	4.25	0.49	31	8.779	16.41	71.98
FBM-46	$1.2×10^6$	13.17	0.49	31	8.925	16.68	73.08
FBM-47	$6.0×10^6$	4.25	0.49	31	10.256	30.18	373.72
FBM-48	$6.0×10^6$	13.17	0.49	31	10.546	31.04	373.72
FBM-49	$1.2×10^7$	4.25	0.49	31	11.502	43.11	722.53
FBM-50	$1.2×10^7$	13.17	0.49	31	11.765	44.09	728.07
FBM-51	$6.0×10^7$	4.25	0.49	31	13.865	99.06	3598.81
FBM-52	$6.0×10^7$	13.17	0.49	31	14.143	101.04	3626.49
FBM-53	$1.2×10^8$	4.25	0.49	31	14.856	122.35	7086.88
FBM-54	$1.2×10^8$	13.17	0.49	31	15.215	125.31	7252.98
FBM-55	300	8.87	0.1	31	1.901	1.93	0.03
FBM-56	300	8.87	0.3	31	1.968	2.00	0.03
FBM-57	600	8.87	0.1	31	2.047	2.09	0.04
FBM-58	600	8.87	0.3	31	2.110	2.15	0.05
FBM-59	1500	8.87	0.1	31	2.444	2.52	0.10
FBM-60	1500	8.87	0.3	31	2.522	2.60	0.11
FBM-61	3000	8.87	0.1	31	2.780	2.90	0.20
FBM-62	3000	8.87	0.3	31	2.883	3.01	0.22
FBM-63	6000	8.87	0.1	31	3.300	3.50	0.39
FBM-64	6000	8.87	0.3	31	3.432	3.64	0.47
FBM-65	$1.5×10^4$	8.87	0.1	31	3.938	4.32	1.04
FBM-66	$1.5×10^4$	8.87	0.3	31	4.036	4.43	1.10
FBM-67	$3.0×10^4$	8.87	0.1	31	4.516	5.14	2.49
FBM-68	$3.0×10^4$	8.87	0.3	31	4.685	5.33	2.59
FBM-69	$6.0×10^4$	8.87	0.1	31	5.357	6.40	4.52
FBM-70	$6.0×10^4$	8.87	0.3	31	5.449	6.51	4.56
FBM-71	$1.5×10^5$	8.87	0.1	31	6.196	8.10	8.61
FBM-72	$1.5×10^5$	8.87	0.3	31	6.297	8.23	8.88
FBM-73	$3.0×10^5$	8.87	0.1	31	7.026	10.08	18.19
FBM-74	$3.0×10^5$	8.87	0.3	31	7.156	10.27	18.37
FBM-75	$6.0×10^5$	8.87	0.1	31	7.585	12.25	35.71
FBM-76	$6.0×10^5$	8.87	0.3	31	7.731	12.48	36.26
FBM-77	$1.2×10^6$	8.87	0.1	31	8.689	16.24	70.87
FBM-78	$1.2×10^6$	8.87	0.3	31	8.715	16.29	71.70
FBM-79	$6.0×10^6$	8.87	0.1	31	10.079	29.66	373.72
FBM-80	$6.0×10^6$	8.87	0.3	31	10.219	30.07	373.72
FBM-81	$1.2×10^7$	8.87	0.1	31	11.339	42.50	722.53
FBM-82	$1.2×10^7$	8.87	0.3	31	11.489	43.06	725.30
FBM-83	$6.0×10^7$	8.87	0.1	31	13.735	98.13	3515.76
FBM-84	$6.0×10^7$	8.87	0.3	31	13.894	99.26	3571.12

FBM-85	1.2×10^8	8.87	0.1	31	14.676	120.87	7059.20
FBM-86	1.2×10^8	8.87	0.3	31	14.834	122.17	7086.88
FBM-87	300	8.87	0.49	40	2.267	2.30	0.11
FBM-88	1500	8.87	0.49	40	2.865	2.95	0.13
FBM-89	3000	8.87	0.49	40	3.267	3.40	0.25
FBM-90	6000	8.87	0.49	40	3.874	4.10	0.52
FBM-91	3.0×10^4	8.87	0.49	40	5.293	5.98	2.95
FBM-92	6.0×10^4	8.87	0.49	40	6.190	7.33	5.12
FBM-93	3.0×10^5	8.87	0.49	40	8.129	11.47	20.05
FBM-94	1.2×10^6	8.87	0.49	40	9.995	18.22	78.52
FBM-95	1.2×10^7	8.87	0.49	40	13.420	48.34	809.62
FBM-96	1.2×10^8	8.87	0.49	40	16.250	149.95	7608.18
FBM-97	60	8.87	0.49	40	1.192	1.20	0.03
FBM-98	92.5	8.87	0.49	40	1.192	1.20	0.04
FBM-99	100	8.87	0.49	40	1.256	1.27	0.04
FBM-100	150	8.87	0.49	40	1.424	1.44	0.06
FBM-101	200	8.87	0.49	40	1.736	1.75	0.06
FBM-102	250	8.87	0.49	40	2.013	1.73	0.09
FBM-103	300	4.25	0.49	40	2.130	2.16	0.03
FBM-104	300	13.17	0.49	40	2.330	2.36	0.05
FBM-105	1500	4.25	0.49	40	2.732	2.81	0.11
FBM-106	1500	13.17	0.49	40	2.951	3.04	0.15
FBM-107	3000	4.25	0.49	40	3.139	3.27	0.23
FBM-108	3000	13.17	0.49	40	3.361	3.50	0.27
FBM-109	6000	4.25	0.49	40	3.746	3.96	0.45
FBM-110	6000	13.17	0.49	40	3.986	4.22	0.55
FBM-111	3.0×10^4	4.25	0.49	40	5.228	5.91	2.87
FBM-112	3.0×10^4	13.17	0.49	40	5.492	6.21	3.00
FBM-113	6.0×10^4	4.25	0.49	40	6.050	7.16	4.98
FBM-114	6.0×10^4	13.17	0.49	40	6.342	7.51	5.21
FBM-115	3.0×10^5	4.25	0.49	40	7.943	11.21	19.62
FBM-116	3.0×10^5	13.17	0.49	40	8.267	11.67	20.17
FBM-117	1.2×10^6	4.25	0.49	40	9.831	17.92	77.86
FBM-118	1.2×10^6	13.17	0.49	40	10.002	18.23	78.97
FBM-119	1.2×10^7	4.25	0.49	40	13.193	47.52	800.74
FBM-120	1.2×10^7	13.17	0.49	40	13.534	48.75	809.62
FBM-121	1.2×10^8	4.25	0.49	40	15.989	147.54	7386.37
FBM-122	1.2×10^8	13.17	0.49	40	16.451	151.80	7652.55
FBM-123	300	8.87	0.1	40	2.104	2.13	0.03
FBM-124	300	8.87	0.3	40	2.155	2.18	0.03
FBM-125	1500	8.87	0.1	40	2.715	2.79	0.10
FBM-126	1500	8.87	0.3	40	2.797	2.88	0.12
FBM-127	3000	8.87	0.1	40	3.081	3.21	0.21
FBM-128	3000	8.87	0.3	40	3.196	3.33	0.24

FBM-129	6000	8.87	0.1	40	3.679	3.89	0.42
FBM-130	6000	8.87	0.3	40	3.802	4.02	0.50
FBM-131	3.0×10^4	8.87	0.1	40	5.057	5.71	2.67
FBM-132	3.0×10^4	8.87	0.3	40	5.242	5.92	2.80
FBM-133	6.0×10^4	8.87	0.1	40	5.988	7.09	4.87
FBM-134	6.0×10^4	8.87	0.3	40	6.096	7.22	4.90
FBM-135	3.0×10^5	8.87	0.1	40	7.814	11.03	19.45
FBM-136	3.0×10^5	8.87	0.3	40	7.981	11.26	19.71
FBM-137	1.2×10^6	8.87	0.1	40	9.717	17.71	76.53
FBM-138	1.2×10^6	8.87	0.3	40	9.753	17.78	77.41
FBM-139	1.2×10^7	8.87	0.1	40	12.988	39.76	798.53
FBM-140	1.2×10^7	8.87	0.3	40	13.198	40.41	802.96
FBM-141	1.2×10^8	8.87	0.1	40	15.773	145.55	7319.83
FBM-142	1.2×10^8	8.87	0.3	40	16.017	147.80	7452.92
EBM Cases ($V_b =$ 1500 m^3, $b =$ 20 m)							
EBM-1	300	8.87	0.49	31	2.686	2.72	0.13
EBM-2	600	8.87	0.49	31	2.876	2.93	0.23
EBM-3	1500	8.87	0.49	31	3.136	3.23	0.33
EBM-4	3000	8.87	0.49	31	3.446	3.60	0.44
EBM-5	6000	8.87	0.49	31	3.756	3.99	0.54
EBM-6	1.5×10^4	8.87	0.49	31	4.721	5.18	1.38
EBM-7	3.0×10^4	8.87	0.49	31	5.123	5.83	2.86
EBM-8	6.0×10^4	8.87	0.49	31	5.552	6.63	5.18
EBM-9	1.5×10^5	8.87	0.49	31	5.918	7.74	9.24
EBM-10	3.0×10^5	8.87	0.49	31	7.260	10.41	18.61
EBM-11	6.0×10^5	8.87	0.49	31	7.960	12.85	36.82
EBM-12	1.2×10^6	8.87	0.49	31	8.931	16.69	72.81
EBM-13	6.0×10^6	8.87	0.49	31	10.405	30.62	373.72
EBM-14	1.2×10^7	8.87	0.49	31	11.667	43.73	725.30
EBM-15	6.0×10^7	8.87	0.49	31	14.125	100.91	3626.49
EBM-16	1.2×10^8	8.87	0.49	31	15.012	123.64	7169.93
EBM-17	300	8.87	0.49	40	2.886	2.92	0.14
EBM-18	1500	8.87	0.49	40	3.398	3.50	0.35
EBM-19	3000	8.87	0.49	40	3.771	3.93	0.46
EBM-20	6000	8.87	0.49	40	4.165	4.41	0.57
EBM-21	3.0×10^4	8.87	0.49	40	5.659	6.40	3.08
EBM-22	6.0×10^4	8.87	0.49	40	6.222	7.37	5.56
EBM-23	3.0×10^5	8.87	0.49	40	8.155	11.51	20.00
EBM-24	1.2×10^6	8.87	0.49	40	9.999	18.23	79.85
EBM-25	1.2×10^7	8.87	0.49	40	13.457	48.47	822.93
EBM-26	1.2×10^8	8.87	0.49	40	16.297	150.38	7741.27

TABLE S5 Summary of large field-scale cases and results

				FBL Cases ($b = $ 50 m)			
Notation	V_0 (m³)	σ	ϕ_f	θ (°)	e	$\hat{L}$	$\Delta\hat{E}_s$
FBL-1	5000	8.87	0.49	31	2.320	2.34	0.06
FBL-2	1.0×10^4	8.87	0.49	31	2.960	3.00	0.12
FBL-3	5.0×10^4	8.87	0.49	31	4.660	4.79	0.69
FBL-4	1.0×10^5	8.87	0.49	31	6.010	6.25	1.38
FBL-5	5.0×10^5	8.87	0.49	31	8.040	8.75	6.64
FBL-6	1.0×10^6	8.87	0.49	31	8.980	10.11	13.45
FBL-7	1.0×10^7	8.87	0.49	31	15.600	21.79	146.17
FBL-8	1.0×10^8	8.87	0.49	31	21.100	47.56	1505.96
FBL-9	1.0×10^9	8.87	0.49	31	25.400	126.14	15170.35
FBL-10	1000	8.87	0.49	31	1.664	1.67	0.01
FBL-11	1500	8.87	0.49	31	1.664	1.67	0.02
FBL-12	2000	8.87	0.49	31	1.664	1.67	0.02
FBL-13	2250	8.87	0.49	31	1.664	1.67	0.02
FBL-14	2450	8.87	0.49	31	1.664	1.67	0.03
FBL-15	2500	8.87	0.49	31	1.664	1.67	0.03
FBL-16	3000	8.87	0.49	31	1.868	1.88	0.03
FBL-17	4000	8.87	0.49	31	2.102	2.12	0.04
FBL-18	5000	4.25	0.49	31	2.192	2.21	0.04
FBL-19	5000	13.17	0.49	31	2.481	2.50	0.06
FBL-20	1.0×10^4	4.25	0.49	31	2.745	2.78	0.10
FBL-21	1.0×10^4	13.17	0.49	31	3.152	3.19	0.17
FBL-22	5.0×10^4	4.25	0.49	31	4.373	4.50	0.56
FBL-23	5.0×10^4	13.17	0.49	31	4.860	5.00	0.76
FBL-24	1.0×10^5	4.25	0.49	31	5.712	5.94	1.20
FBL-25	1.0×10^5	13.17	0.49	31	6.150	6.39	1.43
FBL-26	5.0×10^5	4.25	0.49	31	7.782	8.47	6.09
FBL-27	5.0×10^5	13.17	0.49	31	8.196	8.92	6.81
FBL-28	1.0×10^6	4.25	0.49	31	8.695	9.79	12.13
FBL-29	1.0×10^6	13.17	0.49	31	9.135	10.28	14.01
FBL-30	1.0×10^7	4.25	0.49	31	15.030	20.99	133.99
FBL-31	1.0×10^7	13.17	0.49	31	16.120	22.51	158.90
FBL-32	1.0×10^8	4.25	0.49	31	20.625	46.49	1445.06
FBL-33	1.0×10^8	13.17	0.49	31	21.450	48.35	1544.72
FBL-34	1.0×10^9	4.25	0.49	31	24.469	121.52	14672.06
FBL-35	1.0×10^9	13.17	0.49	31	25.920	128.72	15336.45
FBL-36	5000	8.87	0.1	31	2.023	2.04	0.03
FBL-37	5000	8.87	0.3	31	2.173	2.19	0.04
FBL-38	1.0×10^4	8.87	0.1	31	2.564	2.60	0.07
FBL-39	1.0×10^4	8.87	0.3	31	2.751	2.79	0.10
FBL-40	5.0×10^4	8.87	0.1	31	4.162	4.28	0.41

FBL-41	$5.0×10^4$	8.87	0.3	31	4.379	4.50	0.56
FBL-42	$1.0×10^5$	8.87	0.1	31	5.432	5.65	1.07
FBL-43	$1.0×10^5$	8.87	0.3	31	5.671	5.90	1.17
FBL-44	$5.0×10^5$	8.87	0.1	31	7.456	8.12	5.44
FBL-45	$5.0×10^5$	8.87	0.3	31	7.768	8.46	6.09
FBL-46	$1.0×10^6$	8.87	0.1	31	8.330	9.37	10.85
FBL-47	$1.0×10^6$	8.87	0.3	31	8.623	9.70	11.79
FBL-48	$1.0×10^7$	8.87	0.1	31	14.980	20.92	133.99
FBL-49	$1.0×10^7$	8.87	0.3	31	15.290	21.35	138.42
FBL-50	$1.0×10^8$	8.87	0.1	31	20.400	45.99	1433.99
FBL-51	$1.0×10^8$	8.87	0.3	31	20.690	46.64	1461.67
FBL-52	$1.0×10^9$	8.87	0.1	31	24.750	122.91	14727.42
FBL-53	$1.0×10^9$	8.87	0.3	31	25.090	124.60	14948.89
FBL-54	5000	8.87	0.49	40	2.575	2.60	0.08
FBL-55	$1.0×10^4$	8.87	0.49	40	3.302	3.35	0.17
FBL-56	$5.0×10^4$	8.87	0.49	40	5.205	5.38	0.94
FBL-57	$1.0×10^5$	8.87	0.49	40	6.714	7.03	1.89
FBL-58	$5.0×10^5$	8.87	0.49	40	9.006	9.95	9.19
FBL-59	$1.0×10^6$	8.87	0.49	40	10.064	11.56	18.55
FBL-60	$1.0×10^7$	8.87	0.49	40	16.235	23.84	201.53
FBL-61	$1.0×10^8$	8.87	0.49	40	22.890	56.82	2081.77
FBL-62	$1.0×10^9$	8.87	0.49	40	26.437	150.34	20596.24
FBL-63	1000	8.87	0.49	40	1.192	1.20	0.02
FBL-64	1500	8.87	0.49	40	1.192	1.20	0.02
FBL-65	1750	8.87	0.49	40	1.192	1.20	0.04
FBL-66	2000	8.87	0.49	40	1.365	1.37	0.05
FBL-67	2500	8.87	0.49	40	1.704	1.72	0.06
FBL-68	3000	8.87	0.49	40	2.012	2.03	0.06
FBL-69	4000	8.87	0.49	40	2.365	2.39	0.07
FBL-70	5000	4.25	0.49	40	2.429	2.45	0.06
FBL-71	5000	13.17	0.49	40	2.721	2.75	0.08
FBL-72	$1.0×10^4$	4.25	0.49	40	3.054	3.10	0.13
FBL-73	$1.0×10^4$	13.17	0.49	40	3.501	3.55	0.23
FBL-74	$5.0×10^4$	4.25	0.49	40	4.853	5.01	0.76
FBL-75	$5.0×10^4$	13.17	0.49	40	5.396	5.57	1.04
FBL-76	$1.0×10^5$	4.25	0.49	40	6.377	6.68	1.63
FBL-77	$1.0×10^5$	13.17	0.49	40	6.823	7.14	1.95
FBL-78	$5.0×10^5$	4.25	0.49	40	8.726	9.64	8.42
FBL-79	$5.0×10^5$	13.17	0.49	40	9.184	10.15	9.41
FBL-80	$1.0×10^6$	4.25	0.49	40	9.733	11.18	16.67
FBL-81	$1.0×10^6$	13.17	0.49	40	10.235	11.75	19.27
FBL-82	$1.0×10^7$	4.25	0.49	40	16.739	24.58	183.26
FBL-83	$1.0×10^7$	13.17	0.49	40	18.003	26.44	218.70
FBL-84	$1.0×10^8$	4.25	0.49	40	22.324	55.41	1998.72

FBL-85	1.0×10^8	13.17	0.49	40	23.101	57.34	2131.60
FBL-86	1.0×10^9	4.25	0.49	40	25.537	145.23	19544.29
FBL-87	1.0×10^9	13.17	0.49	40	26.937	153.19	20651.61
FBL-88	5000	8.87	0.1	40	2.239	2.26	0.05
FBL-89	5000	8.87	0.3	40	2.380	2.40	0.06
FBL-90	1.0×10^4	8.87	0.1	40	2.848	2.89	0.09
FBL-91	1.0×10^4	8.87	0.3	40	3.051	3.10	0.13
FBL-92	5.0×10^4	8.87	0.1	40	4.612	4.76	0.56
FBL-93	5.0×10^4	8.87	0.3	40	4.855	5.02	0.76
FBL-94	1.0×10^5	8.87	0.1	40	6.056	6.34	1.46
FBL-95	1.0×10^5	8.87	0.3	40	6.283	6.58	1.59
FBL-96	5.0×10^5	8.87	0.1	40	8.349	9.22	7.42
FBL-97	5.0×10^5	8.87	0.3	40	8.692	9.60	8.42
FBL-98	1.0×10^6	8.87	0.1	40	9.311	10.69	14.95
FBL-99	1.0×10^6	8.87	0.3	40	9.648	11.08	16.17
FBL-100	1.0×10^7	8.87	0.1	40	16.660	24.47	182.71
FBL-101	1.0×10^7	8.87	0.3	40	17.053	25.05	189.91
FBL-102	1.0×10^8	8.87	0.1	40	21.876	54.30	1976.58
FBL-103	1.0×10^8	8.87	0.3	40	22.327	55.42	2015.33
FBL-104	1.0×10^9	8.87	0.1	40	25.799	146.72	19599.65
FBL-105	1.0×10^9	8.87	0.3	40	26.257	149.32	20042.58

EBL Cases ($V_b = 10^5$ m^3, $b = 50$ m)

EBL-1	5000	8.87	0.49	31	3.75	3.78	0.32
EBL-2	1.0×10^4	8.87	0.49	31	4.42	4.48	0.64
EBL-3	5.0×10^4	8.87	0.49	31	6.22	6.39	1.53
EBL-4	1.0×10^5	8.87	0.49	31	6.925	7.20	2.36
EBL-5	5.0×10^5	8.87	0.49	31	8.25	8.98	7.14
EBL-6	1.0×10^6	8.87	0.49	31	9.25	10.41	15.56
EBL-7	1.0×10^7	8.87	0.49	31	15.8	22.07	158.90
EBL-8	1.0×10^8	8.87	0.49	31	21.2	47.79	1572.40
EBL-9	1.0×10^9	8.87	0.49	31	25.5	126.64	15557.92
EBL-10	5000	8.87	0.49	40	4.078	4.12	0.41
EBL-11	1.0×10^4	8.87	0.49	40	4.815	4.89	0.84
EBL-12	5.0×10^4	8.87	0.49	40	6.697	6.92	2.03
EBL-13	1.0×10^5	8.87	0.49	40	7.606	7.96	3.16
EBL-14	5.0×10^5	8.87	0.49	40	9.243	10.21	9.74
EBL-15	1.0×10^6	8.87	0.49	40	10.301	11.83	21.21
EBL-16	1.0×10^7	8.87	0.49	40	16.428	24.13	216.48
EBL-17	1.0×10^8	8.87	0.49	40	22.977	57.03	2153.75
EBL-18	1.0×10^9	8.87	0.49	40	26.509	150.75	20651.61

TABLE S6 Parameters used in empirical relationship[2] for debris flow efficiency

The efficiency of debris flow is the inverse of the friction coefficient (i.e., $e = \mu^{-1}$), which

is defined by Lucas et al. (2014) as follows,

$$\mu = \frac{\mu_0 - \mu_w}{(1 + |U|/U_w)} + \mu_w \tag{S1}$$

where μ_0 and μ_w are the static and thermally weakened friction coefficients, and U

is the maximum debris flow velocity, and U_w is a characteristic velocity for the onset of

dramatic weakening, controlled by competition between frictional heating and heat

conduction. According to Lucas et al. (2014), μ_0 varies from 0.5 to 1.2, μ_w ranges

from 0.03 to 0.16, whereas U_w varies from 0.8 m/s to 8.5 m/s , all of which depend on

the volume of debris flow. In the present study, μ_w is kept constant ($\mu_w = 0.03$); the

values of μ_0 and U_w are listed below.

FBS Cases ($U_w = 4$ m/s)					
$\theta = 31°$			$\theta = 40°$		
Notation	$V_0 (\text{m}^3)$	μ_0	Notation	$V_0 (\text{m}^3)$	μ_0
FBS	6	0.99	FBS-57	6	0.99
FBS-1	12	0.99	FBS-58	12	0.99
FBS-2	25	0.99	FBS-59	25	0.99
FBS-3	50	0.98	FBS-60	50	0.98
FBS-4	100	0.98	FBS-61	100	0.98
FBS-5	200	0.98	FBS-62	200	0.98
FBS-6	400	0.98	FBS-63	400	0.98
FBS-7	800	0.97	FBS-64	800	0.97
FBS-8	1200	0.97	FBS-65	1200	0.97
FBS-9	1600	0.97	FBS-66	1600	0.97
FBS-10	2	1.09	FBS-67	1	1.09
FBS-11	2.5	1.09	FBS-68	1.33	1.09
FBS-12	3	1.07	FBS-69	1.4	1.07
FBS-13	3.5	1.05	FBS-70	1.6	1.05
FBS-14	4	1.03	FBS-71	1.8	1.03
FBS-15	4.5	1.01	FBS-72	2	1.01
FBS-16	5	1.00	FBS-73	3	1.00
FBM Cases ($U_w = 6$ m/s)					

	$\theta=$ 31°			$\theta=$ 40°	
Notation	V_0 (m³)	μ_0	Notation	V_0 (m³)	μ_0
FBM-1	300	1.2	FBM-87	300	1.075
FBM-2	600	1.2	FBM-88	1500	1.05
FBM-3	1500	1.16	FBM-89	3000	1.05
FBM-4	3000	1.1	FBM-90	6000	1.05
FBM-5	6000	1	FBM-91	3.0×10^4	1
FBM-6	1.5×10^4	0.95	FBM-92	6.0×10^4	0.95
FBM-7	3.0×10^4	0.9	FBM-93	3.0×10^5	0.875
FBM-8	6.0×10^4	0.85	FBM-94	1.2×10^6	0.8
FBM-9	1.5×10^5	0.8	FBM-95	1.2×10^7	0.8
FBM-10	3.0×10^5	0.8	FBM-96	1.2×10^8	0.8
FBM-11	6.0×10^5	0.8	FBM-97	60	1.2
FBM-12	1.2×10^6	0.8	FBM-98	92.5	1.2
FBM-13	6.0×10^6	0.8	FBM-99	100	1.15
FBM-14	1.2×10^7	0.8	FBM-100	150	1.15
FBM-15	6.0×10^7	0.8	FBM-101	200	1.1
FBM-16	1.2×10^8	0.8	FBM-102	250	1.1
FBM-17	30	1.2			
FBM-18	50	1.2			
FBM-19	100	1.2			
FBM-20	152.5	1.2			
FBM-21	175	1.2			
FBM-22	250	1.2			

FBL Cases ($U_w=$ 8.5 m/s)

	$\theta=$ 31°			$\theta=$ 40°	
Notation	V_0 (m³)	μ_0	Notation	V_0 (m³)	μ_0
FBL-1	5000	1.15	FBL-54	5000	1.1
FBL-2	1.0×10^4	1.1	FBL-55	1.0×10^4	1
FBL-3	5.0×10^4	0.8	FBL-56	5.0×10^4	0.75
FBL-4	1.0×10^5	0.6	FBL-57	1.0×10^5	0.6
FBL-5	5.0×10^5	0.6	FBL-58	5.0×10^5	0.525
FBL-6	1.0×10^6	0.55	FBL-59	1.0×10^6	0.5
FBL-7	1.0×10^7	0.5	FBL-60	1.0×10^7	0.5
FBL-8	1.0×10^8	0.5	FBL-61	1.0×10^8	0.5
FBL-9	1.0×10^9	0.5	FBL-62	1.0×10^9	0.5
FBL-10	1000	1.2	FBL-63	1000	1.2
FBL-11	1500	1.2	FBL-64	1500	1.2
FBL-12	2000	1.15	FBL-65	1750	1.2
FBL-13	2250	1.15	FBL-66	2000	1.15
FBL-14	2450	1.15	FBL-67	2500	1.15
FBL-15	2500	1.15	FBL-68	3000	1.1
FBL-16	3000	1.15	FBL-69	4000	1.1
FBL-17	4000	1.15			